iScience

CellPress
OPEN ACCESS

Article

Numerical study on atomization characteristics of biomimetic evaporation tube in micro turbine engine

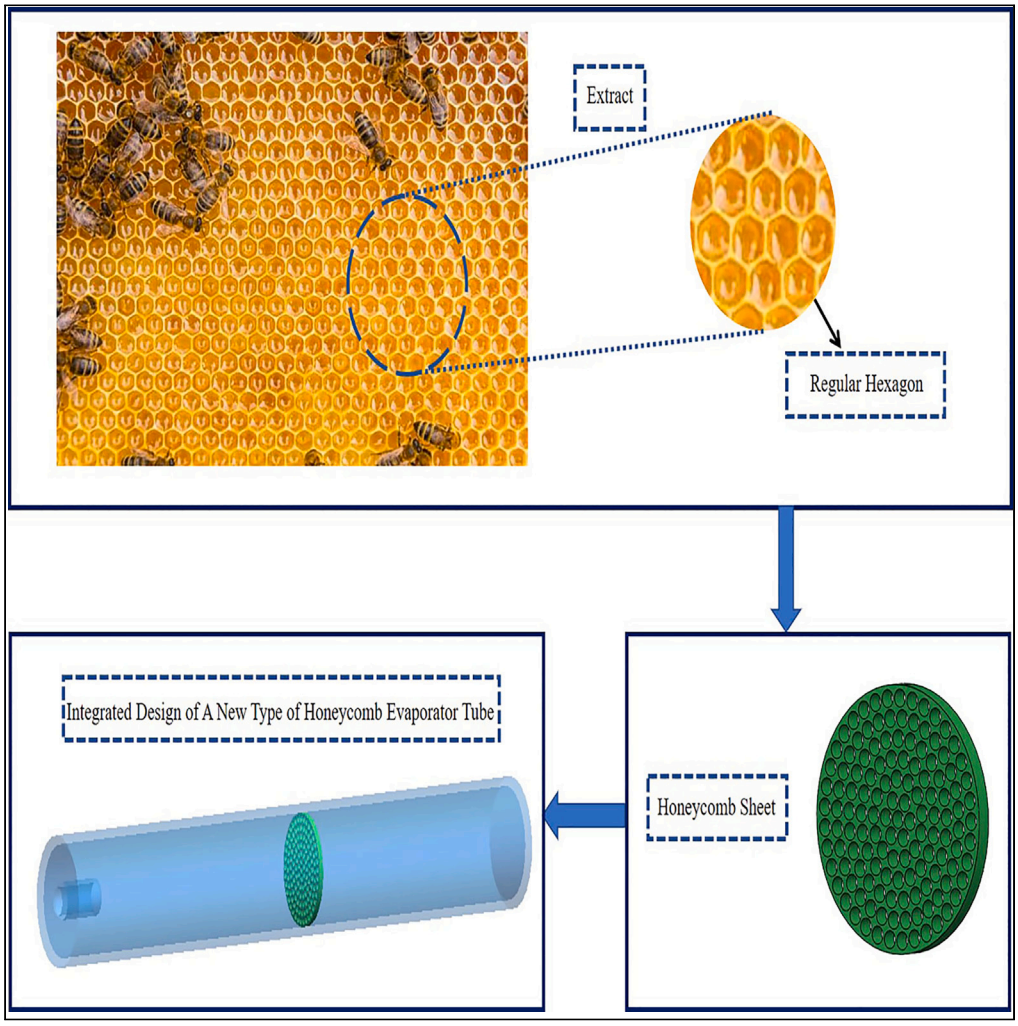

Xinming Zhang, Qingyu Zhang, Guowei Li, Jing Hu

hujing@cust.edu.cn

Highlights

Foundational role of the evaporation tube in the combustion chamber design

Theoretical study of evaporation and atomization in the tube

Proposing a bionic-inspired tube with a honeycomb sheet

Study atomization in traditional and new tube setups

Zhang et al., iScience 27, 109144
March 15, 2024
https://doi.org/10.1016/j.isci.2024.109144

iScience

CellPress
OPEN ACCESS

Article

Numerical study on atomization characteristics of biomimetic evaporation tube in micro turbine engine

Xinming Zhang,[1,2,3,4] Qingyu Zhang,[1,2,5] Guowei Li,[1,2] and Jing Hu[1,2,6,*]

SUMMARY

A micro turbine engine's thrust relies on combustion chamber efficiency, closely tied to the design of its evaporation tube. This study thoroughly investigates evaporation and atomization processes within the tube, introducing a pioneering bionic-inspired structure. Integrating a honeycomb sheet into the traditional tube, both configurations undergo a comparative analysis. Results show a direct correlation between elevated air temperatures and reduced fuel droplet diameters, leading to increased fuel evaporation rates. The bionic tube, with a 1mm-thick honeycomb sheet, 0.6 mm aperture diameter, and 3 sheets, significantly improves fuel droplet atomization and evaporation compared to the conventional design. This research holds broader significance in understanding and enhancing micro turbine engine performance.

INTRODUCTION

In recent years, driven by the evolution of national defense strategies and the rapid advancement of the civil market economy, aviation equipment has assumed a significant role. This is particularly evident through the emergence of micro devices, which have not only garnered increased attention within both domestic and foreign military sectors but have also ushered in an extended sphere for potential development.[1–6] Micro turbine engines (MTEs) showcase advantages including lightweight construction, high energy density within a compact form, and an impressive thrust-to-weight ratio. Consequently, they are extensively employed in diverse applications, encompassing both military and civilian unmanned aircraft.[7–9] The intrinsic advantages of MTEs have garnered substantial attention from scholars, positioning them as a central focus of research on both domestic and international fronts.[10,11] The combustion chamber assumes a pivotal role within MTE, exerting direct influence over the engine's performance. Traditionally, the combustion chamber is classified into three distinct structures: the single-tube combustion chamber, the ring-tube combustion chamber, and the annular combustion chamber. Similarly, the gas flow pattern manifests in three forms: straight-flow combustion chamber, the folded combustion chamber, and the reverse-flow combustion chamber. Collectively, these distinctions define the operational framework and potential outcomes of MTE.[12] The prevailing development direction in high-performance micro turbine engines is characterized by straight-flow annular combustion chambers.[13] The advantages of the straight-flow annular combustion chamber structure encompass uniform combustion, high efficiency, reduced emissions, minimized vibration and noise levels, and enhanced system stability. The specific benefits are discussed in the following: 1. Simplicity: the straightforward design of the straight-flow annular combustion chamber translates to lower manufacturing and maintenance costs. Its simplicity also facilitates experiments and research. 2. Stable gas flow mode: thanks to its unique design, the gas flow mode in the straight-flow annular combustion chamber remains relatively stable. This ensures uniform mixing and complete combustion of fuel, leading to heightened thermal efficiency and reduced pollutant emissions. 3. High combustion efficiency: a notable advantage of the straight-flow annular combustion chamber is its elevated combustion efficiency. This is achieved by pre-mixing fuel and air at the nozzle, creating a more homogeneous mixture within the combustion chamber. This uniform mixture contributes to improved combustion speed and efficiency. As the engine's fundamental component, the combustion chamber necessitates engineering that ensures its resilience against high temperatures, increased pressures, and swiftly changing dynamic conditions.[14–16] In the realm of fuel atomization and evaporation, typically, evaporator tubes with simple structures and low supply pressures are employed. The configuration of the evaporator tube directly impacts the primary recirculation zone and flow dynamics within the combustion chamber, thus emphasizing the significance of designing the evaporator tube structure and delving into its laws governing evaporation and atomization.[17] Zhang et al. [18] investigated two evaporative tube fuel supply devices for stationary vortex combustion chambers, analyzing atomization and evaporation performance under various conditions. Xing et al. [19] addressed fuel burning issues in the outer ring cooling chamber during stationary vortex combustion tests by optimizing the evaporation tube's straight section, and

[1]Chongqing Research Institute, Changchun University of Science and Technology, Chongqing 401120, China
[2]School of Mechatronical Engineering, Changchun University of Science and Technology, Changchun 130022, China
[3]School of Mechatronic Engineering and Automation, Foshan University, Foshan 528225, China
[4]Precision Machining and Special Machining Innovation Team, Guangdong Education Department, Foshan 528225, China
[5]College of Control Science and Engineering, Bohai University, Jinzhou 121013, China
[6]Lead contact
*Correspondence: hujing@cust.edu.cn
https://doi.org/10.1016/j.isci.2024.109144

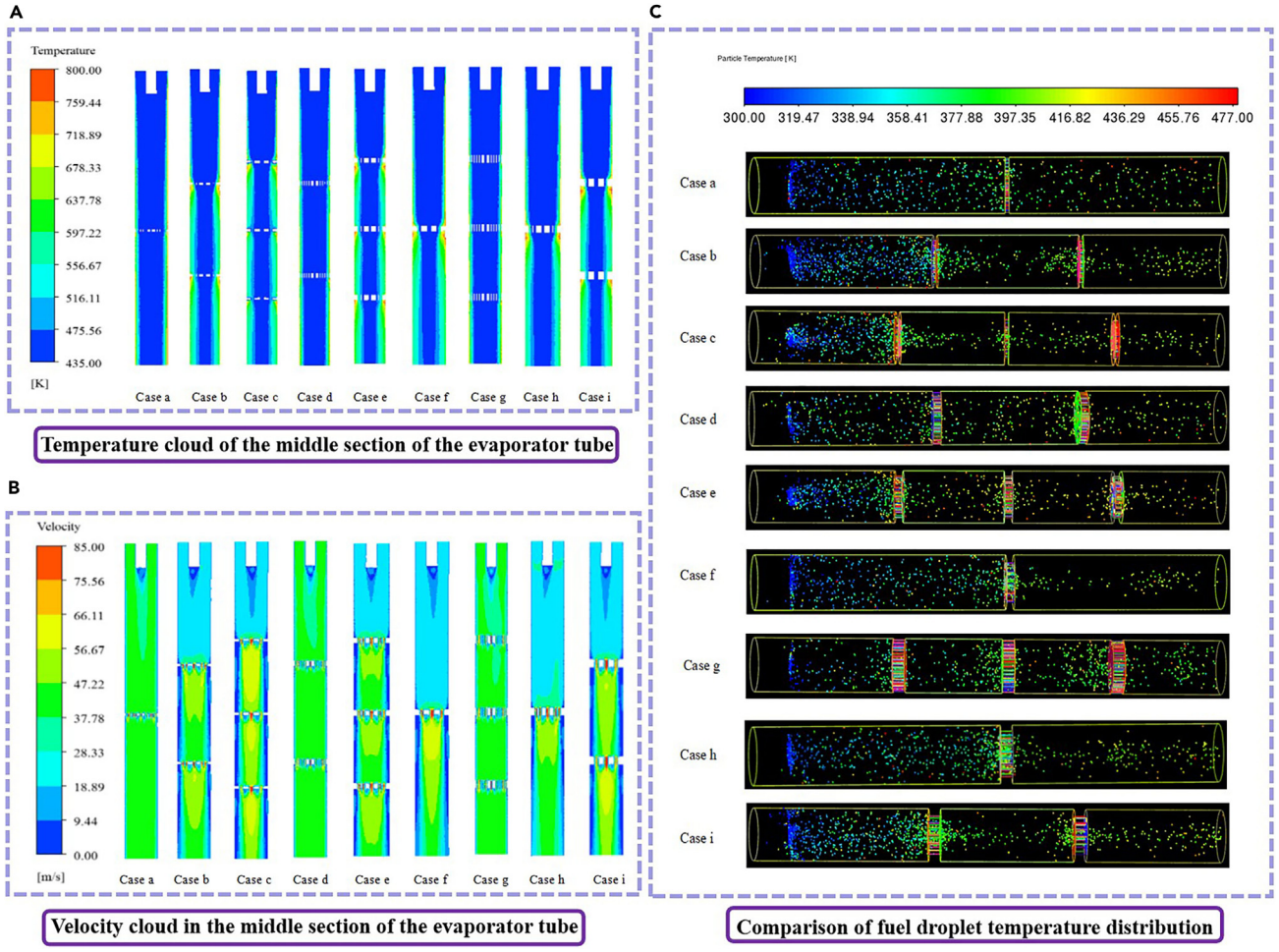

Figure 1. Cloud map of temperature, velocity, and fuel droplet temperature distribution in the middle section of the evaporator tube

(A) Temperature cloud of the middle section of the evaporate tube.

(B) Velocity cloud in the middle section of the evaporate tube.

(C) Comparison of fuel droplet temperature distribution.

identifying factors affecting combustion efficiency. Zhu et al.[20] experimentally investigated the variation pattern of fuel evaporation rate in a T-shaped evaporation tube using indirect measurement methods. Results showed an increase in evaporation rate with higher gas-oil ratios, stabilizing after reaching a critical value. Liu et al.[21] enhanced the surface shape of corrugated pipes, introducing a sinusoidal corrugated heat exchange pipe. Experimental findings on a sleeve-type heat transfer platform revealed significantly improved heat transfer efficiency compared to straight pipes. Gawron et al.[22] investigated the combustion chamber evaporation tube of a micro engine, establishing an experimental platform for measuring MTE pollutant emissions. They studied the impact of mixing hole position and size on combustion chamber evaporation tube performance and pollutant emission levels using experimental and numerical simulation methods.

This article proposes a novel honeycomb evaporation tube structure, inspired by bionics, to address low evaporation and atomization efficiency in traditional tubes. In-depth research on the relationship between tube parameters, incoming flow, and fuel atomization was conducted, focusing on factors such as honeycomb sheet thickness, opening size, and sheet number. Identified key factors provide a theoretical basis for enhancing fuel atomization and evaporation, supporting advanced MTE combustion chamber design and improving combustion efficiency.

RESULTS

Effect of honeycomb sheet on air temperature inside the evaporator tube

Analyzing the temperature distribution at the middle interface of the evaporator tube, as depicted in Figure 1A (case a), (case d), and (case g), reveals that under similar conditions of opening diameter, honeycomb sheet thickness, and number of honeycomb sheets, the temperature alteration in the wall and inner tube is relatively inconspicuous. The wall temperature and internal tube temperature fluctuations remain

Table 1. Orthogonal test analysis table

Programmatic	A	B	C	Evaporation rate (%)
a	1	1	1	7.30
b	1	2	2	13.42
c	1	3	3	30.14
d	2	1	2	18.59
e	2	2	3	41.74
f	2	3	1	9.03
g	3	1	3	28.27
h	3	2	1	15.14
i	3	3	2	16.61
K1	50.86	54.16	31.47	–
K2	69.36	70.30	48.62	–
K3	60.02	55.78	100.15	–
k1	16.95	18.05	10.49	–
k2	23.12	23.43	16.21	–
k3	20.01	18.59	33.38	–
Range	6.17	5.38	22.89	
Optimal solution	A2	B2	C3	

minimal. Notably, in scenarios characterized by a smaller opening diameter, the incoming air experiences enhanced stability, contributing to a relatively modest overall internal temperature within the evaporator tube. Consequently, this setup exerts a limited influence on the evaporation rate and behavior of fuel droplets.

Examining Figure 1A (case b), (case c), (case e), (case f), (case h), and (case i), it becomes apparent that the presence of honeycomb holes at specific locations is prone to generating localized regions of elevated temperature. During such instances, an increase in the diameter of the openings relative to previous scenarios, along with variations in honeycomb sheet size, thickness, and number of holes, can collectively influence the internal air temperature within the evaporator tube.

The introduction of honeycomb holes induces a distinct cyclonic effect in the incoming air, leading to an augmented heat exchange area. This phenomenon contributes to a measured increase in air temperature. Specifically, in comparison to schemes c and g, scheme e exhibits a broader coverage of elevated temperatures with a more uniform temperature rise, thus yielding a more effective evaporation outcome.

Incorporating a thinner honeycomb sheet, a smaller opening diameter, and a greater number of honeycomb sheets results in a larger heat transfer surface area within the evaporator tube. Additionally, the presence of honeycomb holes fosters cyclonic activity, which plays a pivotal role in enhancing convective heat transfer. Both of these factors collectively contribute to improved evaporation performance.

Effect of honeycomb on the air velocity inside the evaporation tube

A comprehensive analysis of Figure 1B (case a), (case d), and (case g) underscores the presence of a relatively uniform flow rate within the evaporator tube. This is particularly evident in cases where the honeycomb sheet opening diameter and incoming gas flow rate are relatively small.

Examining Figure 1B (case b), (case c), (case e), (case f), (case h), and (case i), it is observed that in the initial phase, as the incoming air encounters the honeycomb sheet, velocity disparities emerge, visually depicted through the cloud diagrams. This distinction arises due to the given boundary conditions of inlet and outlet pressures in the calculation process. Varying honeycomb sheet thickness, opening diameter, and number of holes result in differing flow resistance performance, which subsequently impacts the inlet and outlet velocities for each scenario. Specifically, thicker honeycomb sheet thickness, smaller opening diameter, and a greater number of honeycomb sheets contribute to higher flow resistance, resulting in lower average inlet and outlet velocities. This trend aligns with the corresponding inlet air flow pattern.

The introduction of honeycomb sheets and holes contributes to the creation of distinct high-speed and low-speed zones within the tube. This phenomenon induces relative motion between the air and droplets, amplifying shear fragmentation effects. As a result, the atomization of fuel droplets is enhanced, owing to the intensified interaction facilitated by these airflow patterns.

Effect of honeycomb sheet on the atomization and evaporation of fuel droplets

Figure 1C depict the temperature distribution of fuel droplets within the evaporation tube for one of the nine scenarios. Typically, fuel droplets start at lower temperatures and progressively warm up over time as atomization occurs. Consequently, droplet diameter decreases, and the droplets undergo movement within the evaporation tube.

Table 2. Comparative analysis of the calculation results of the traditional evaporator tube and the new evaporator tube

Programmatic	Evaporation rate (%)	Outlet SMD (μm)	Air flow (g/s)	Average outlet temperature (K)
E	41.74	29.9	2.34	515.4
J	2.09	68.3	3.44	479.0

Upon the close examination of the figures, a distinct pattern emerges. Fuel droplets exhibit a gradual temperature increase along the tube axis. The overall distribution is notably influenced by both honeycomb holes and gravity. Particularly, droplets are concentrated primarily near the inception point of the honeycomb holes, where the influence of air cyclones propels their motion and gradual dispersion.

Orthogonal test analysis

The orthogonal analysis method is employed, utilizing the evaporation rate as a singular indicator, and the results are presented in Table 1. K1, K2, and K3 represent the sums of evaporation rates corresponding to the first, second, and third levels of factors A, B, and C, respectively. k1, k2, and k3 are calculated as the means of the three values in the respective rows of K1, K2, and K3, where k1 = K1/3.

The extreme deviation is defined as the absolute difference between the largest and smallest values among the three numbers in the same column. This deviation quantifies the magnitude of variation within a specific factor. By calculating the absolute difference between the largest and smallest values within the same column, we assess the variability across different levels of the factor. Furthermore, this deviation is computed for k1, k2, and k3 within the same column, resulting in the absolute value of the difference between the largest and smallest values. A higher extreme deviation signifies a more pronounced influence of the factor on the evaporation rate. Notably, the column exhibiting the greatest extreme difference denotes the key factor exerting the most substantial impact on the evaporation rate.

Analyzing the table above reveals the varying degrees of influence that each factor exerts on the evaporation rate, ranked in descending order as follows: B (diameter of the open hole), A (thickness of the honeycomb sheet), and C (number of honeycomb sheets). Thicker honeycomb sheet thickness and a larger number of honeycomb sheets correspond to a higher evaporation rate, albeit with increased air flow resistance. Notably, the table indicates that the diameter of honeycomb sheet openings holds the smallest extreme difference at 5.38, signifying a relatively minor impact on the evaporation rate. Thus, it cannot be conclusively inferred that an increased number of apertures in the honeycomb sheet inherently leads to an enhanced evaporation rate. Through the lens of orthogonal analysis, the optimal selection scheme is identified as A2B2C3, corresponding to scheme e. Increasing the number of honeycomb cells can enhance the atomization process of fuel; however, it's not necessarily true that more honeycomb cells always lead to better performance. In fact, there is an optimal value for the number of honeycomb panels. Beyond this threshold, increasing the number of honeycomb panels may no longer yield significant performance improvements and could even lead to performance degradation. This occurs because, after reaching a certain number of honeycomb panels, the atomization effect of the fuel approaches an optimal state, and further increases have a limited impact on improving atomization. Additionally, an excess of honeycomb cells may heighten the complexity and cost of the system, potentially resulting in issues such as increased flow resistance and pressure loss. Therefore, when selecting the number of honeycomb cells, comprehensive considerations are necessary, including factors such as the atomization effect, system complexity, and cost. Determining the optimal number of honeycomb cells through numerical simulation is crucial to achieve the best atomization effect and overall system performance.

Comparison of the performance of traditional straight evaporator tubes and new evaporator tubes

The same numerical model and boundary conditions were employed to perform numerical calculations on the traditional straight evaporator tube without fins, designated as scheme j. This scheme was then compared and analyzed against scheme e, which represents the optimal outcome from the orthogonal test, as illustrated in Table 2, Figure 1A (case e), Figure 1B (case e), and Figure 1C (case e). An examination of the pertinent data in the table reveals that the numerical simulation method employed in this study yielded an evaporation rate of only 2.09% for the traditional evaporator tube. In contrast, scheme e, incorporating a honeycomb structure through innovative design, achieved a significantly higher evaporation rate of 41.74%. The evaporation rate stands as a pivotal core performance metric, and the incorporation of the honeycomb structure has led to a substantial enhancement in the evaporator tube's performance. The average Sauter mean diameter of fuel droplets at the outlet cross-section has decreased from 68.3 μm to 29.9 μm, underscoring the role of the honeycomb sheet in improving the atomization performance of the evaporator tube. Additionally, the average outlet temperature has risen from 478.99K to 515.41K, indicative of the honeycomb structure's contribution to intensified heat exchange between the tube wall and the surrounding air, thereby facilitating the efficient evaporation of fuel droplets.

However, it's worth noting that the innovative honeycomb structure design does introduce a partial negative influence in the form of potential tube clogging, which can lead to reduced airflow rates under the same differential pressure. The transition from scenario j to scenario e saw an air flow reduction from 3.44 g/s to 2.34 g/s, indicating a decrease of 30.8%, highlighting the more pronounced clogging effect. Despite this, in the context of designing a combustion chamber, utilizing a combustion chamber based on the traditional straight tube design, with modifications limited to the evaporator tube, allows for changes in tube diameter and honeycomb aperture size to maintain the new evaporator tube's airflow rate on par with the original design. In light of this, the obstructive impact of the new honeycomb structure should The inspiration for honeycomb sheet design predominantly stems from the not be considered a hindrance to the evaporator tube's performance, but rather a means to elevate and optimize its overall functionality.

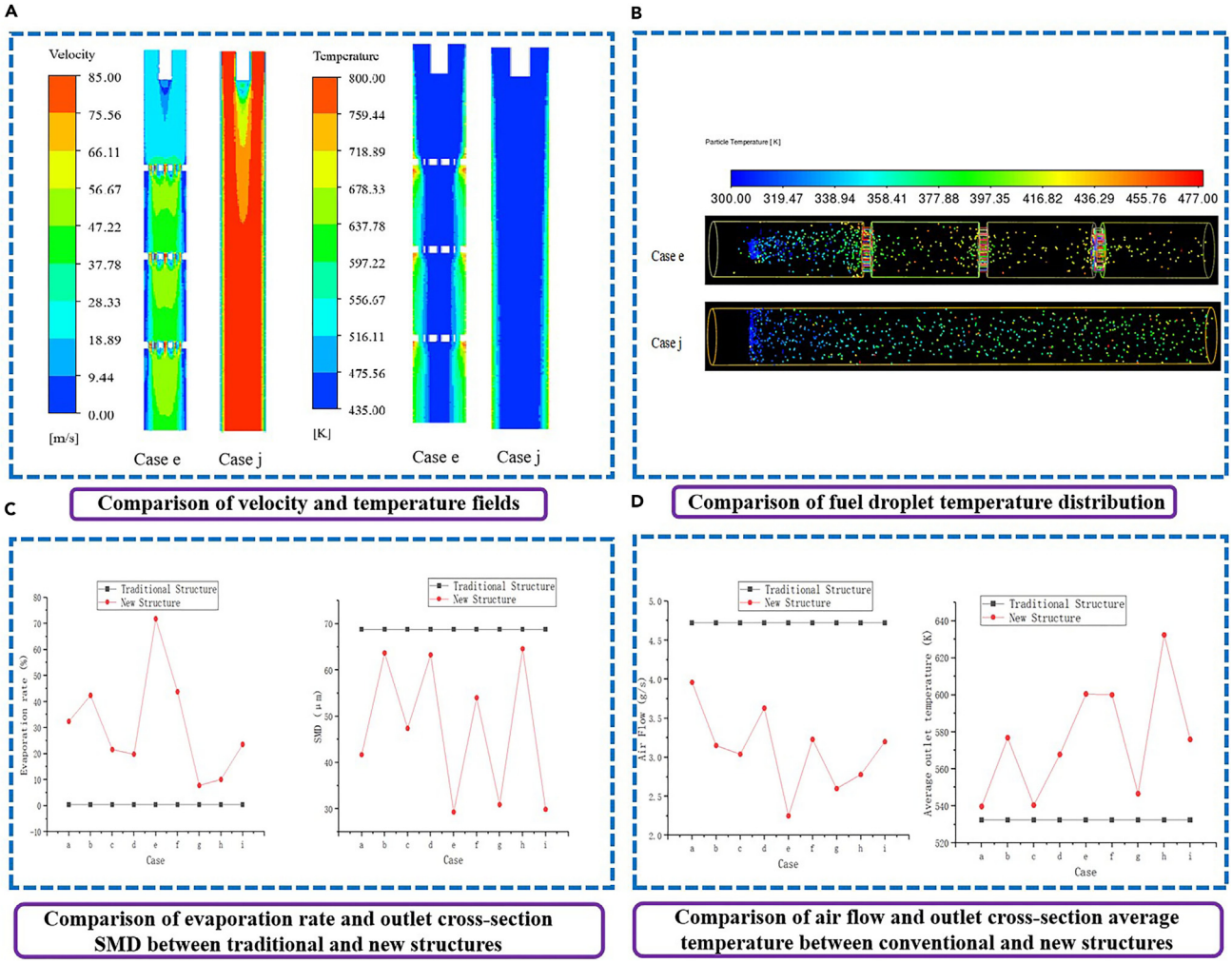

Figure 2. Comparison of evaporation rate, outlet cross-section SMD, airflow, and average temperature of outlet cross-section between traditional and new structures

(A) Comparison of velocity and temperature fields.

(B) Comparison of fuel droplet temperature distribution.

(C) Comparison of evaporation rate and outlet cross-section SMD between traditional and new structures.

(D) Comparison of air flow and outlet cross-section average temperature between conventional and new structures.

Honeycomb structure exhibits superior fuel droplet atomization and evaporation efficiency compared to other biomimetic evaporation tube structures. Practical limitations may include manufacturing complexity, high costs, performance constraints under specific conditions, stability and durability concerns, and potential fluctuations under certain working conditions.

Upon analyzing Figures 2A and 2B, a discernible pattern emerges: the temperature of the internal air within the tube experiences a gradual increase in alignment with the flow direction. From the perspective of atomization, the traditional evaporator tube exhibits low flow resistance and high air velocity, resulting in a uniform speed distribution throughout. Conversely, the introduction of the new honeycomb structure disrupts the incoming air, inducing regions of turbulent velocity alterations within the tube. This turbulence prompts a substantial rise in the gas-liquid relative velocity, thereby magnifying the aerodynamic forces acting on droplets. As a consequence, droplets are more susceptible to fragmentation, rendering the environment conducive to effective atomization.

Within the confines of the traditional evaporation tube (scheme j), a discernible trend emerges as the high-temperature region gradually extends from the tube wall toward the center. This development, however, encounters limitations in terms of heat transfer effectiveness, as noticeable alterations primarily occur in proximity to the tube wall and extend only moderately into the surrounding air. Fuel droplets predominantly congregate within the central region, distancing themselves from the tube wall surface. Consequently, the central area experiences less significant heating from the surrounding air, leading to a more gradual temperature increase. Regrettably, this slower temperature rise fails to reach the requisite evaporation threshold, resulting in a diminished evaporation rate.

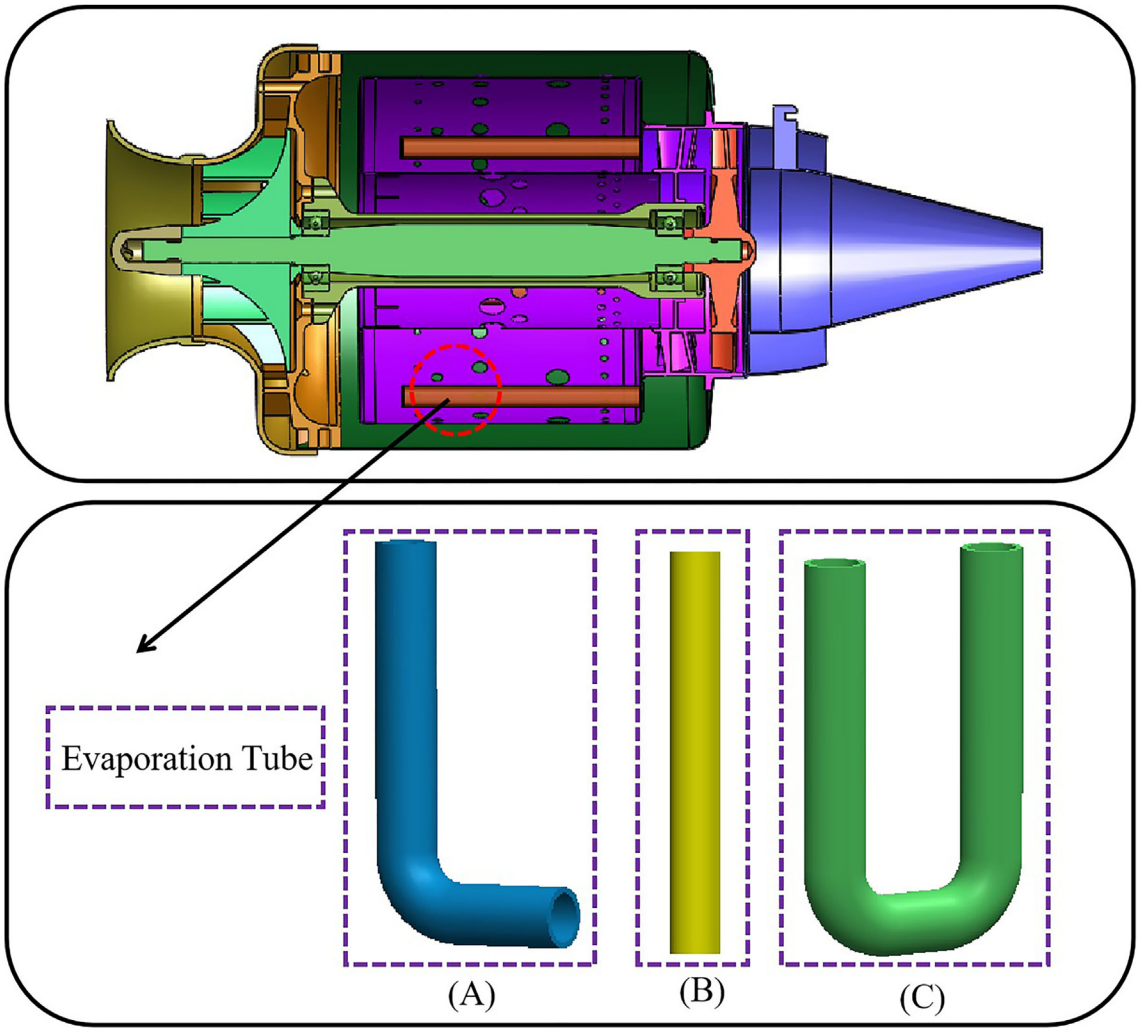

Figure 3. Common evaporator tube structure diagram

(A) L-type evaporator tube model drawing.

(B) Model diagram of a straight evaporator tube.

(C) U-shaped evaporator tube model drawing.

Upon implementing the novel structural design, two notable enhancements become evident. Firstly, the introduction of the honeycomb structure generates air perturbations, thereby inducing a significant rise in the average temperature within the central region of the tube and at the outlet. This effect results in a more uniform temperature distribution, promoting favorable conditions for fuel droplet atomization and subsequently boosting the evaporation rate. Secondly, the presence of the honeycomb structure enables fuel droplets to directly collide with the honeycomb sheet's surface. This collision facilitates enhanced heat absorption and direct heat transfer between the fuel droplets and the wall, particularly due to the honeycomb structure's influence. As a result, the fuel droplets gain direct exposure to the elevated temperature zone along the tube wall, contributing to improved evaporation efficiency.

The analysis presented in Figure 2C illustrates a clear superiority of each scenario involving the novel honeycomb sheet structure within the evaporator tube when compared to the conventional counterpart. The optimal scheme, denoted as e, emerges as the front runner, showcasing the highest evaporation rate and the smallest Sauter Mean Diameter (SMD), thus exemplifying superior performance among all considered schemes. Furthermore, as depicted in Figure 2D, the optimal scheme e exhibits a lower air flow rate and a relatively higher average outlet temperature. This temperature increase is attributed to the incorporation of the new honeycomb sheet structure. To summarize the findings from the aforementioned scenarios, it can be concluded that the introduction of a honeycomb sheet structure within the evaporator tube leads to performance enhancement. Notably, the presence of an optimal honeycomb structure, as evidenced in specific cases, can maximize the performance benefits of the evaporator tube.

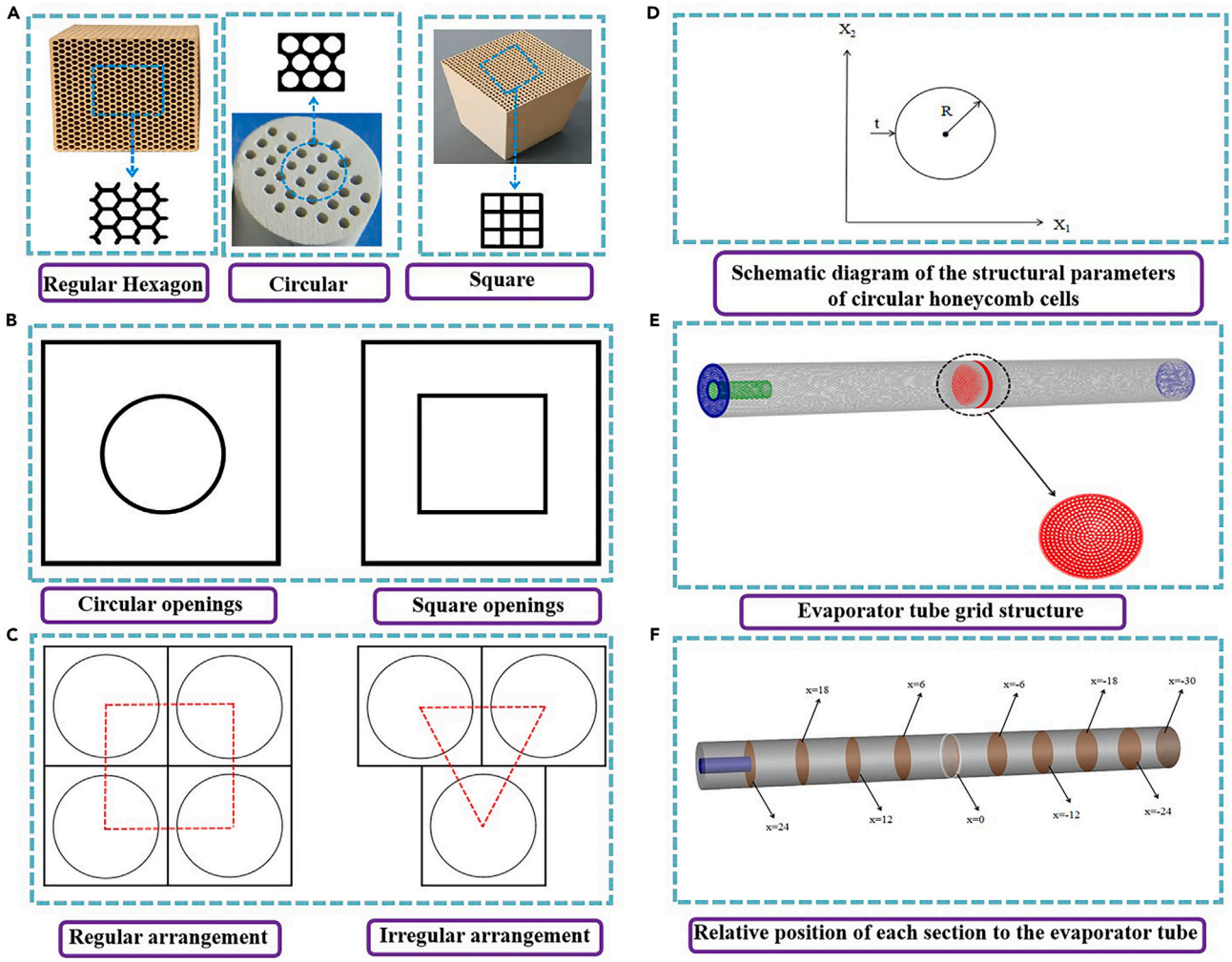

Figure 4. Schematic diagram of different aperture shapes, grid structure of evaporator tubes, and relative positions of each section

(A) Schematic diagram of different aperture shapes.

(B) Circular openings and square openings.

(C) Regular arrangement and irregular arrangement.

(D) Schematic diagram of the structural parameters of circular honeycomb cells.

(E) Evaporator tube grid structure.

(F) Relative position of each section to the evaporator tube.

DISCUSSION

Selection of common types of evaporation tubes and biomimetic models

Evaporator tubes are commonly found in three configurations: straight, L-shaped, and U-shaped, as illustrated in Figure 3. While these configurations serve similar roles during evaporation, subtle differences exist in layout and fluid dynamics.

The straight tube structure is renowned for its simplicity and compactness, often being the preferred choice. Firstly, its simple and compact design makes it one of the most straightforward and space-saving options. This structure connects directly to the fuel nozzle, eliminating the need for complex pipeline arrangements or connectors. This minimalist design not only simplifies manufacturing and maintenance but also reduces the time and cost of design and assembly. Secondly, the straight pipe structure experiences lower pressure loss, a key consideration for MTE. Typically, it produces smaller pressure losses compared to other designs. The combustion flow path of the straight tube structure is simple, avoiding complex bending or branching, thereby reducing fluid dynamic resistance and minimizing energy loss. Finally, the straight tube structure plays a pivotal role in minimizing fuel residence time, a primary factor for ensuring MTE stability. The residence time of fuel in a straight pipe significantly influences the evaporation rate and uniformity of fuel transfer, underscoring the importance of this structural choice. It's worth noting that straight tube configurations usually require shorter evaporator tube lengths. Compared to more complex structures, fuel stays in the straight tube for a shorter period, alleviating fluctuations in fuel content and reducing potential issues of uneven evaporation. In

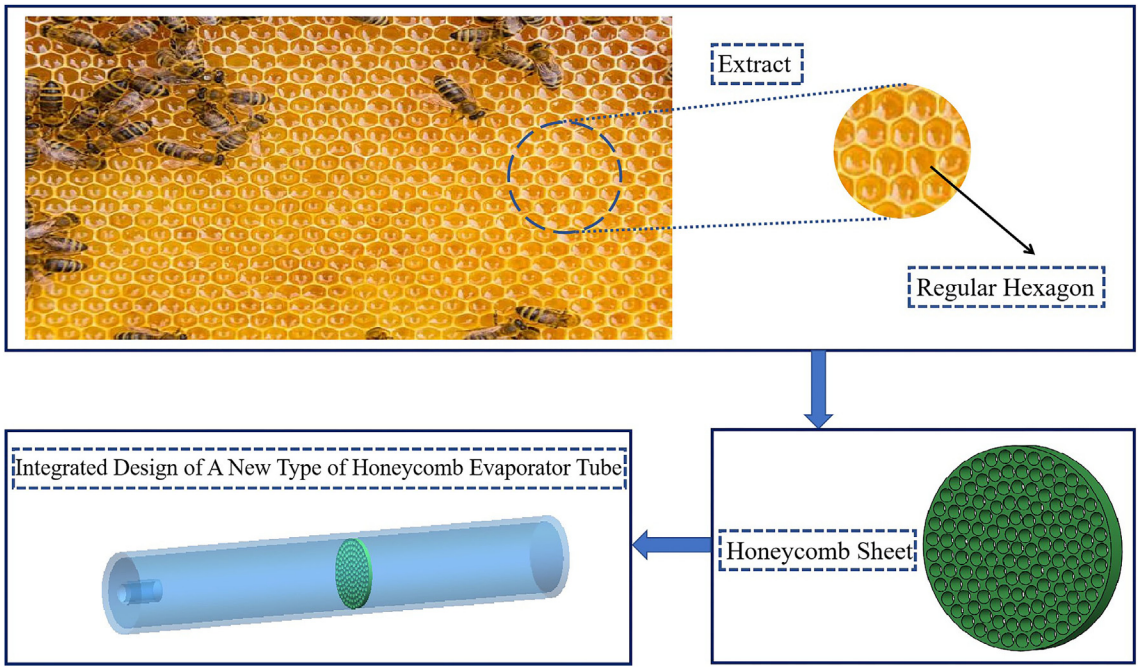

Figure 5. Schematic illustration of biomimetic honeycomb sheet structure

contrast, the configuration of U-shaped and L-shaped pipes is more complex and requires additional space. For specific applications, they may lack the flexibility to adapt to complex environments, and their flow performance may not be as efficient as other pipe shapes.[20]

To further enhance the evaporation rate and fuel atomization performance of the straight tube structure, the incorporation of a honeycomb sheet structure is introduced. This augmentation aims to elevate evaporation efficiency and bolster combustion stability.

The honeycomb structure finds its roots in bionics, and today it stands as a prominent constituent within aerospace composites. This structural pattern has permeated numerous airframe components, including floors, side panels, baggage racks, and ceilings. Offering attributes distinct from conventional structures, the honeycomb design boasts a comprehensive high-performance profile characterized by lightweight, low density, elevated strength, robust rigidity, impact resistance, vibration damping, and acoustic and thermal insulation.

Furthermore, the honeycomb structure offers unique advantages such as a substantial specific surface area, heightened heat storage and release rates, an expansive effective circulation area, and minimal resistance loss. These advantages have propelled its widespread adoption on the international stage. The most common honeycomb structures encompass square, hexagonal, and circular patterns, as depicted in Figure 4A.

The inspiration for honeycomb sheet design predominantly stems from the intricate structure of beehives. Honeycomb materials offer exceptional attributes, including remarkable fracture toughness, effective vibration damping, impressive impact resistance, and noise reduction capabilities. As a result, these materials have found extensive applications across diverse industries, encompassing aerospace, satellite technology, maritime vessels, railway vehicles, electronic communications, and even nano-manufacturing processes.[23–25] Over the course of several decades, honeycomb structures have witnessed substantial progress across multiple facets, including structural design, resistance to damage, and the utilization of materials.[26–28] The reasons for choosing and implementing the honeycomb structure within a straight evaporator tube are as follows: 1. Enhanced Heat Transfer Efficiency: The honeycomb structure comprises numerous small channels or pores,

Table 3. Factors influencing the performance of circular openings over square openings

Geometric symmetry	Stress concentration relief	Uniform deformation	Shape affects folding path	Structural continuity
Circular structures' geometric symmetry promotes even stress distribution, slows local deformation, ensuring overall structural stability	Circular holes are more effective in alleviating stress concentration, reducing local stress, and preventing local instability and fracture	Circular holes' distribution facilitates uniform deformation during compression, promoting overall regularity and stability	Circular structure shapes influence folding paths, easing the formation of regular and stable folding shapes during compression deformation	Circular structure shapes impact the folding path, facilitating the formation of regular and stable folding shapes during compression deformation

Table 4. Physical parameters of honeycomb body

Material	Densities ρ (kg/m^3)	Isobaric specific heat C_P (J/Kg·K)	Thermal conductivity λ (W/m·K)
Mullite	2500	500	2.14–4.37

effectively amplifying the surface area of the evaporator tube and furnishing additional heat transfer routes. 2. Improved Mass Transfer: Beyond its heat transfer capabilities, the honeycomb structure also bolsters mass transfer processes. 3. Strength and Structural Stability: Comprised of interconnected small holes or channels, the honeycomb structure forms a robust framework.[29]

On the contrary, alternative configurations such as U-type, L-type, and the like, may exhibit certain limitations or reasons for their inapplicability.[20,29]

(1) Elaborate Piping Arrangements: Other structures often necessitate more intricate piping layouts, entailing a higher number of connections and branches in their design. This augmented complexity not only escalates fabrication and assembly intricacies but also potentially introduces additional pressure losses and heightened hydrodynamic resistance.
(2) Inferior Heat Transfer Efficiency: Unlike the honeycomb structure, other designs might struggle to deliver comparable heat transfer efficiency due to their relatively diminutive surface areas. This disparity can constrain the overall performance and efficiency of the evaporator tube.

In conclusion, opting for the honeycomb structure within a straight evaporator tube offers a multitude of advantages. This choice not only enhances heat transfer efficiency and mass transfer effectiveness but also upholds ample strength and structural stability. Consequently, it contributes to the further enhancement of evaporation efficiency and fuel atomization effects. The ultimate selection of integrating the honeycomb structure with the straight evaporator tube emerges as a promising and effective design approach. Figure 5 illustrates the implementation of a novel honeycomb structure within the evaporator tube.

Analysis of factors influencing the honeycomb design of wall openings

An analysis is conducted to explore the influence of various opening shapes on the average compression force experienced by the honeycomb structure. This assessment takes into comprehensive account the potential deformation arising within the evaporation tube under fluid impact. As depicted in Figure 4B, a comparison is drawn between two distinct open hole models. Typically, all wall-opened honeycomb structures tend to undergo gradual compression and compaction.

In honeycomb structures featuring different hole-side ratios, the folding centers of wall-opened honeycombs predominantly align with the center of the respective open hole. Furthermore, the lengths of the folded cells exhibit minimal alteration during the compression deformation process. Notably, in the course of compression deformation, cellular structures characterized by round holes yield more regular and stable folded configurations. Conversely, wall-opened cellular structures with square holes tend to exhibit more irregular folded states.[30,31] Table 3 details factors favoring circular over square openings. For the honeycomb sheet, the chosen material's physical parameters are provided in Table 4. For the current study, an $L_9(3^4)$ orthogonal table is utilized. Three honeycomb sheet shape control parameters are identified as influencing factors, each with three levels. The resultant scheme is outlined in Table 5. The calculated outcomes of the evaporator tubes for the nine distinct scenarios are presented in Table 6.

As per pertinent research, it is evident that wall surface openings in the form of round holes tend to exhibit greater stability compared to square holes. Furthermore, the stress-strain curve of honeycomb structures during the compression process demonstrates reduced fluctuation within the impact compression phase. It is worth noting that the stability of honeycomb structures with round holes is slightly superior to those with square holes.[32–34] In this study, the choice is made to employ a circular honeycomb structure. The design encompasses both

Table 5. Table of experimental program design for shape control factors

Programmatic	A	B	C	Honeycomb sheet thickness (mm)	Hole diameter (mm)	Number of honeycomb pieces (pcs)
A	1	1	1	0.5	0.4	1
b	1	2	2	0.5	0.6	2
c	1	3	3	0.5	0.8	3
d	2	1	2	1	0.4	2
e	2	2	3	1	0.6	3
f	2	3	1	1	0.8	1
g	3	1	3	1.5	0.4	3
h	3	2	1	1.5	0.6	1
i	3	3	2	1.5	0.8	2

Table 6. Calculation results of evaporator tube for each program

Programmatic	Evaporation rate (%)	Outlet SMD (μm)	Air flow (g/s)	Average outlet temperature (K)
a	7.30	51.5	2.77	481.5
b	13.42	53.6	2.58	497.1
c	30.14	37.1	2.44	507.1
d	18.59	30.4	2.45	483.6
e	41.74	29.9	2.34	515.4
f	9.03	35.5	2.86	504.4
g	28.17	35.1	2.42	505.0
h	15.14	34.1	2.89	489.5
i	16.61	35	2.55	503.2

regularly arranged and irregularly arranged circular honeycomb structures, as depicted in Figure 4C. The schematic representation of its structural cell parameters can be observed in Figure 4D.

During the reliability validation at higher velocities, the circular hole honeycomb structure is constructed using parallel circular tubes. Its crushing process mirrors that of individual circular tubes, where the circular hole honeycomb undergoes crushing from the outer surface, a phase referred to as the platform stage. Hu et al.[35] employed a theoretical approach to analyze circular honeycomb structures subjected to anisotropic impact loading. They introduced an expression to forecast the average stress within circular honeycomb configurations:

$$\sigma = \frac{C_1}{K} \cdot \left(\frac{T}{D}\right)^{n_1} \cdot \sigma_S + \frac{\pi\left(\frac{T}{D}\right)}{K(1 - C_2)\sqrt{\frac{T}{D}}} \cdot \rho_s \cdot V^2 \quad \text{(Equation 1)}$$

Formula: C_1, C_2K, n_1, all are constants; T is the cytosolic wall thickness; D is the diameter of the circular honeycomb cell element; ρ_S is the density of the material; σ_s is the yield stress; V is the dynamic compression speed. For regular arrangements, the various constants are $C_1 = 5.89 C_2 = 1.259$, $K = 1.1$, $n_1 = 1.3686$;

for irregular arrangements $C_1 = 5.86$, $C_2 = 1.129 K = 0.786$, $n_1 = 1.3611$.

To maximize the opening rate and enhance heat exchange efficiency in the new structure, this article incorporates both regular and irregular arrangements. Optimization involves adjusting element shape, size, and spacing, and strategically distributing regular and irregular elements. Regular arrangement maximizes opening area, improving heat exchange and ensuring uniform liquid distribution. Irregular openings increase liquid disturbance, forming a complex flow pattern, enhancing surface area, and improving evaporation efficiency. Systematic research identifies the optimal law for the maximum opening rate, providing a tailored structural solution for specific design requirements. Honeycomb sheet openings: 0.4 mm (133), 0.6 mm (40), 0.8 mm (20).

Conclusion

This article presents the design of a novel evaporator tube structure inspired by honeycomb bionic characteristics. The study involves the establishment of flow field and fuel evaporation models, aimed at exploring the intricate processes of fuel atomization and evaporation within the evaporator tube. By examining various parameters of the honeycomb sheet, the impact on fuel atomization and evaporation within a singular evaporator tube is thoroughly investigated. The key conclusions drawn from this study are as follows.

(1) The thickness of the honeycomb sheet plays a pivotal role in influencing fuel atomization and evaporation. Optimal atomization and evaporation performance are achieved with a suitable thickness. In this study, a thickness of 1 mm proves to be a more suitable choice, as it enhances the evaporation effectiveness of fuel droplets.

(2) Variations in the diameter of the honeycomb sheet openings lead to corresponding changes in incoming flow rates, exerting a significant influence on fuel droplet atomization and evaporation. Larger aperture diameters within the honeycomb structure result in higher flow rates passing through the cross-section per unit of time within the evaporation tube. A smaller diameter of the evaporation tube leads to a higher incoming flow rate, causing a greater disparity in gas-liquid relative velocities and increased perturbation, thus enhancing atomization effects. In this study, the selection of a 0.4 mm opening diameter yields improved evaporation performance.

(3) The increased number of honeycomb pieces corresponds to heightened flow resistance, resulting in reduced average velocities at both the inlet and outlet. This behavior aligns with the trend exhibited by the inlet air flow. This phenomenon creates distinct high-speed and low-speed zones within the tube, promoting relative velocities between air and droplets. This variance intensifies shear fragmentation, thereby enhancing fuel droplet atomization. In the simulation experiments conducted herein, a configuration involving three honeycomb pieces was selected, yielding improved evaporation effects.

Limitations of the study

Complexity and Cost: The new design introduces increased complexity in manufacturing and maintenance, potentially leading to elevated costs. Specifically, the process of manufacturing and installing the honeycomb sheets may require additional processes and resources.

STAR★METHODS

Detailed methods are provided in the online version of this paper and include the following:

- KEY RESOURCES TABLE
- RESOURCE AVAILABILITY
  - Lead contact
  - Materials availability
  - Data and code availability
- METHOD DETAILS
  - Modeling of heat transfer inside the evaporator tube
  - Physical modeling and meshing
  - Calculation methods
  - Boundary conditions
  - Orthogonal design
  - Selection of eigenfaces
  - Comparison of the performance of evaporator tubes in different structural states

ACKNOWLEDGMENTS

This research is supported by the Chongqing Natural Science Foundation of China under Contract No. CSTB2022NSCQ-MSX1332, and Scientific Research Project of Education Department of Guangdong Province (2022KCXTD029).

AUTHOR CONTRIBUTIONS

X. M., Z. supervised the article and funding acquisition; Q. Y., Z. collected data and wrote the article; G. W., L. analyzed data; J. H. conceived the idea funding acquisition and visualization; and all authors discussed the results and approved the article.

DECLARATION OF INTERESTS

The authors declare no competing interests.

Received: October 17, 2023
Revised: January 26, 2024
Accepted: February 1, 2024
Published: February 6, 2024

REFERENCES

1. Azadi, G., Zand, Z., Mousazade, Y., Bagheri, R., Cui, J.F., Song, Z.L., Bikas, R., Wozniak, K., Allakhverdiev, S., and Najafpour, M. (2019). A tetranuclear nickel (II) complex for water oxidation: meeting new challenges. Int. J. Hydrogen Energy *44*, 2857–2867. https://doi.org/10.1016/j.ijhydene.2018.12.059.
2. Cho, S., Ma, J., and Yakimenko, O. (2022). Aerial multi-spectral AI-based detection system for unexploded ordnance. Defence Technol. *27*, 24–37. https://doi.org/10.1016/j.dt.2022.12.002.
3. Voskuijl, M. (2022). Performance analysis and design of loitering munitions: A comprehensive technical survey of recent developments. Defence Technol. *18*, 325–343. https://doi.org/10.1016/j.dt.2021.08.010.
4. Karneeb, J., Floyd, M.W., Moore, P., and Aha, D.W. (2018). Distributed discrepancy detection for a goal reasoning agent in beyond-visual-range air combat. AI Commun. *31*, 181–195. https://doi.org/10.3233/AIC-180757.
5. Wang, M., Wang, L., Yue, T., and Liu, H. (2020). Influence of unmanned combat aerial vehicle agility on short-range aerial combat effectiveness. Aero. Sci. Technol. *96*, 105534. https://doi.org/10.1016/j.ast.2019.105534.
6. Yang, C., Wu, H., Du, J., Zhang, H., and Yang, J. (2022). Full-engine simulation of micro gas turbine based on time-marching throughflow method. Appl. Therm. Eng. *217*, 119213–119225. https://doi.org/10.1016/j.applthermaleng.2022.119213.
7. Perpignan, A., Sacomano Filho, F.L., and Krieger, G. (2012). Design analysis of a micro gas turbine combustion chamber burning natural gas. In ASME Turbo Expo, Copenhagen, Denmark, *5*, pp. 797–805. https://doi.org/10.1115/GT2012-69180.
8. Topal, A., Catori, C., Çağan, L., Uslu, S., Turan, Ö., and Pişkin, A. (2014). Exit temperature profile measurement and CFD comparisons on small scale turbojet combustor with air blast atomizer configuration. In AIAA/ASME/SAE/ASEE joint propulsion conference, *2* (Cleveland, OH: American Institute of Aeronautics and Astronautics), pp. 3525–3539. https://doi.org/10.2514/6.2014-3525.
9. Cao, H.L., and Xu, J.L. (2007). Thermal performance of a micro-combustor for micro-gas turbine system. Energy Convers. Manag. *48*, 1569–1578. https://doi.org/10.1016/j.enconman.2006.11.022.
10. Tuttle, S., Hinnant, K., and Vick, M. (2017). Preliminary design, ignition, and fuel injection for a high temperature recuperated microturbine combustor. In Proceedings of the ASME Turbine Technical Conference and Exposition (Charlotte, USA, 4A: ASME), pp. 63165–63174. https://doi.org/10.1115/GT2017-63165.
11. Liu, C.K., and Li, Y.R. (2018). Performance simulation model of millimeter-scale micro turbine engine. J. Beijing Univ. Aeronaut.

Astronaut. *44*, 1430–1437. https://doi.org/10.13700/j.bh.1001-5965.2017.0566.

12. Yang, B., Hu, L., Ping, W., Roy, R., and Gupta, A.K. (2021). Boron-nitride nanosheet-based thermal barrier coating for Micro-combustor performance improvement. J. Energy Resour. Technol. *144*, 062106-062109. https://doi.org/10.1115/1.4052734.
13. Clarke, J.S., and Jackson, S.R. (1964). In General consideration in the design of combustion chambers for aircraft and industrial gas turbines (Sae World Congress & Exhibition), pp. 96–115. https://doi.org/10.4271/640009.
14. Hosseini, S.E. (2019). Micro-power generation using micro-turbine (moving) and thermophotovoltaic (non-moving) systems. Proc. Inst. Mech. Eng. Part A Journal of Power and Energy *233*, 1085–1101. https://doi.org/10.1177/0957650919841958.
15. Yang, M., Wu, X., Zhou, W., Liu, X., Qiang, R., and Huang, F. (2023). Experimental study on effects of different water flow rates on heat transfer characteristics of evaporator. J. Phys, Conf. Ser. *2418*, 012003-012009. https://doi.org/10.1088/1742-6596/2418/1/012003.
16. Fan, W.J., Kong, Z.J., Li, J.B., Yang, M.L., and Yi, Q. (2007). Performance of pulverization and evaporation of new type evaporating fuel inject equipment. J. Propuls. Technol. *28*, 244–247. https://doi.org/10.13675/j.cnki.tjjs.2007.03.005.
17. Tan, W.L., Fan, W.J., Zhang, T., Wang, W.J., and Zhang, R.C. (2012). Performance test of micro turbojet engines evaporator and numerical simulation of the combustor. J. Aero. Power *27*, 861–867. https://doi.org/10.13224/j.cnki.jasp.2012.04.022.
18. Zhang, R.C., FAN, W.J., and Song, S.W. (2011). Atomization and evaporation performance experiment of evaporating tube for trapped vortex combustor. J. Aero. Power *26*, 2495–2502. https://doi.org/10.13224/j.cnki.jasp.2011.11.028.
19. Xing, F., Zhang, S., and Zheng, Y. (2011). An optimal study on a TVC evaporation tube using moving particle semi-implicit method. J. Propuls. Technol. *32*, 339–342. https://doi.org/10.13675/j.cnki.tjjs.2011.03.013.
20. Zhu, J., Guo, X.H., Lin, Y.Z., and Xu, G.Q. (2007). Experimental research on vaporization rate of micro "T"-vaporizer. J. Aero. Power *22*, 1273–1278. https://doi.org/10.13224/j.cnki.jasp.2007.08.014.
21. Liu, J., Zhang, H.P., and Pei, W. (2005). The experimental research on the heat transfer properties of sinusoidal corrugated tubes. China Petroleum Machinery *33*, 1–3. https://doi.org/10.3969/j.issn.1001-4578.2005.03.001.
22. Gawron, B., and Białecki, T. (2016). Measurement of exhaust gas emissions from miniature turbojet engine. Combustion Engines *167*, 58–63. https://doi.org/10.19206/CE-2016-406.
23. Feng, G., Li, S., Xiao, L., and Song, W. (2021). Energy absorption performance of honeycombs with curved cell walls under quasi-static compression. Int. J. Mech. Sci. *210*, 106746–106767. https://doi.org/10.1016/j.ijmecsci.2021.106746.
24. Natarajan, E., Freitas, L.I., Santhosh, M.S., Markandan, K., Majeed Al-Talib, A.A., and Hassan, C.S. (2023). Experimental and numerical analysis on suitability of S-Glass-Carbon fiber reinforced polymer composites for submarine hull. Defence Technol. *19*, 1–11. https://doi.org/10.1016/j.dt.2022.06.003.
25. Zhou, S., Xie, L., Zhang, X., Yan, M., Zeng, H., Liang, K., Jiang, L., and Kong, B. (2023). Super-assembled Multi-level asymmetric mesochannels for coupled accelerated dual-ion selective transport. Adv. Mater. *35*, 2208903–2208913. https://doi.org/10.1002/adma.202208903.
26. Yan, M., Liu, T., Li, X., Zhou, S., Zeng, H., Liang, Q., Liang, K., Wei, X., Wang, J., Gu, Z., et al. (2022). Soft patch interface-oriented superassembly of complex hollow nanoarchitectures for smart dual-responsive nanospacecrafts. J. Am. Chem. Soc. *144*, 7778–7789. https://doi.org/10.1021/jacs.2c01096.
27. Zhou, S., Xie, L., Li, X., Huang, Y., Zhang, L., Liang, Q., Yan, M., Zeng, J., Qiu, B., Liu, T., et al. (2021). Interfacial super-assembly of ordered mesoporous carbon-silica/AAO hybrid membrane with enhanced permselectivity for temperature- and pH-sensitive smart ion transport. Angew. Chem. *60*, 26167–26176. https://doi.org/10.1002/ange.202110731.
28. Greco, F. (2013). A study of stability and bifurcation in micro-cracked periodic elastic composites including self-contact. Int. J. Solids Struct. *50*, 1646–1663. https://doi.org/10.1016/j.ijsolstr.2013.01.036.
29. Lin, Y.Z., Liu, J., Xu, Q.H., and Wei, W.B. (2006). Study on vaporization rate of a mini Γ-vaporizer under atmospheric pressure condition. J. Aero. Power *5*, 843–847. https://doi.org/10.13224/j.cnki.jasp.2006.05.011.
30. Gong, S.G., Xiao, Q.C., and Xie, G.L. (2021). Study on mechanical properties of out-of-plane compression for honeycomb structure with holes in wall. Mechanical Science and Technology for Aerospace Engineering *40*, 1293–1298. https://doi.org/10.13433/j.cnki.1003-8728.20200193.
31. Qi, C., Jiang, F., and Yang, S. (2021). Advanced honeycomb designs for improving mechanical properties: A review. Compos. B Eng. *227*, 109393–109416. https://doi.org/10.1016/j.compositesb.2021.109393.
32. Ren, Y.L., Jiang, H.Y., Jin, Q.D., and Zhu, G.H. (2021). Crashworthiness of bio-inspired auxetic reentrant honeycomb with negative poisson's ratio. Acta Aeronautica Astronautica Sinica *42*, 314–324. https://doi.org/10.7527/S1000-6893.2020.23978.
33. Shen, Z.F., Zhang, X.C., Bai, J.P., and Wu, H.X. (2020). Dynamic response characteristics of re-entrant circular honeycombs with negative poisson's ratio. J. Vib. Shock *39*, 89–95. https://doi.org/10.13465/j.cnki.jvs.2020.18.011.
34. Xu, P., Yang, C., Peng, Y., Yao, S., Zhang, D., and Li, B. (2016). Crash performance and multi-objective optimization of a gradual energy-absorbing structure for subway vehicles. Int. J. Mech. Sci. *107*, 1–12. https://doi.org/10.1016/j.ijmecsci.2016.01.001.
35. Hu, L.L., He, X.L., Wu, G.P., and Yu, T. (2015). Dynamic crushing of the circular-celled honeycombs under out-of-plane impact. Int. J. Impact Eng. *75*, 150–161. https://doi.org/10.1016/j.ijimpeng.2014.08.008.
36. Zhang, K.P. (2019). CFD simulation and experimental verification for one subway air-conditioning condensing unit. Refrig. Air Cond. *19*, 45–49. https://doi.org/10.3969/j.issn.1009-8402.2019.10.011.
37. Li, C., Lei, Y.B., and Pan, X.F. (2018). Experiment on evaporation efficiency of vaporizer and numerical simulation of two-phase flow in vaporizer. J. Aero. Power *33*, 2877–2884. https://doi.org/10.13224/j.cnki.jasp.2018.12.008.
38. Zhang, Q., Kou, R., Li, C.C., Chen, S., Wang, R., and Yang, X.Z. (2019). Numerical Study on fuel atomization and evaporation characteristics of evaporative tubes in micro combustor. Aeroengine *45*, 1–5. https://doi.org/10.13477/j.cnki.aeroengine.2019.01.001.

STAR★METHODS

KEY RESOURCES TABLE

REAGENT or RESOURCE	SOURCE	IDENTIFIER
Deposited data		
Numerical Simulation Dataset	This paper	N/A
Software and algorithms		
Ansys-fluent 19.2	ANSYS	https://www.ansys.com/

RESOURCE AVAILABILITY

Lead contact

Further information and requests for resources should be directed to and will be fulfilled by the lead contact, Jing Hu (hujing@cust.edu.cn).

Materials availability

This study did not generate new unique materials.

Data and code availability

- All data reported in this paper will be shared by the lead contact upon request.
- This paper does not report the original code.
- Any additional information required to reanalyze the data reported in this paper is available from the lead contact upon request.

METHOD DETAILS

Modeling of heat transfer inside the evaporator tube

The governing equations governing the flow of fluid within an evaporator tube encompass the continuity equation for incompressible flow in three dimensions with constant physical properties, the Navier-Stokes equation for momentum conservation, and the energy conservation equation.[36]

The continuity equation:

$$\frac{\partial u}{\partial x}+\frac{\partial v}{\partial y}+\frac{\partial w}{\partial z}=0 \quad \text{(Equation 2)}$$

in Equation 2, u, v, w are the components of velocity in the x, y, z directions, respectively.

Momentum conservation equation:

$$u\frac{\partial U_i}{\partial x}+v\frac{\partial U_i}{\partial y}+w\frac{\partial U_i}{\partial z}=-\frac{1}{\rho}\frac{\partial p}{\partial x}+v\left(\frac{\partial^2 U_i}{\partial x^2}+\frac{\partial^2 U_i}{\partial y^2}+\frac{\partial^2 U_i}{\partial z^2}\right) \quad \text{(Equation 3)}$$

in Equation 3: ρ is the fluid density; p is the pressure; v is the kinematic viscosity of the fluid; U_i is the velocity component in the i-direction.

The energy conservation equation:

$$u\frac{\partial t}{\partial x}+v\frac{\partial t}{\partial y}+w\frac{\partial t}{\partial z}=a\left(\frac{\partial^2 t}{\partial x^2}+\frac{\partial^2 t}{\partial y^2}+\frac{\partial^2 t}{\partial z^2}\right) \quad \text{(Equation 4)}$$

in Equation 4: is the heat diffusion coefficient; is the fluid temperature.

In incompressible flow, Navier-Stokes equations are employed to characterize fluid motion, applicable to incompressible flows like those in evaporator tubes. Additionally, for processes involving phase and density changes, such as atomization and evaporation, the mass transfer model is crucial. This model captures diffusion and transport of substances in the fluid, addressing interactions during phase and density changes. In the evaporation of fuel, transitioning from liquid to gas, these equations effectively describe the associated processes.

Physical modeling and meshing

Drawing upon relevant existing data models, a solitary evaporator tube structure is extracted and subsequently refined and optimized. This process yields the requisite geometric model essential for numerical simulation analysis.

For numerical simulation calculations, a non-structural mesh division approach is implemented. This entails encrypting the nozzle outlet and concentrating grid modifications in localized areas of structural change. Furthermore, the wall of the pipe is similarly subjected to grid

enhancement. To ensure result accuracy, multiple verifications of grid independence are performed. Upon reaching a grid count of approximately two million, a relative optimal solution is achieved. The chosen mesh configuration employs a hybrid structure comprising hexahedral meshes in the central region and tetrahedral meshes in the proximity of the walls, as illustrated in Figure 4E.

The evaporator tube, with a total length of 60 mm and an inner diameter of 6 mm, features a 5 mm separation between the nozzle outlet and the evaporator tube inlet. Notably, a single honeycomb sheet is positioned at the center of the evaporator tube. Positioning the honeycomb panel at the evaporator's center aims for uniform evaporation, ensuring consistent temperature and humidity distribution. This minimizes temperature gradients, preventing localized overheating or overcooling. The panel's position significantly influences simulation outcomes for evaporation performance and temperature distribution. Placing honeycomb panels differently yields varied hydrodynamic effects and heat transfer characteristics. Opting for center placement maximizes impact across the entire system, providing a comprehensive evaluation of global performance.

Calculation methods

The computational fluid dynamics (CFD) analyses in this study are conducted utilizing the commercial software FLUENT 19.2. The flow field in the evaporator tube is solved with a pressure-based implicit segregated solver. A standard K-ε turbulence model with a wall function near the wall is selected to describe turbulent structure and energy dissipation. Introducing turbulent kinetic energy and dissipation rate enhances simulation accuracy for vortex and energy transfer processes in turbulent fluids. In Fluent, choose a suitable turbulence model like the k-ε Model, configure parameters, and set initial and boundary conditions for accurate turbulence simulation. Pressure-velocity coupling uses the SIMPLE algorithm, and equation discretization follows a 2nd-order upwind format to ensure robust results.

For the nozzle atomization model, the Discrete Phase Model (DPM) is employed. The secondary fragmentation model adopts the Wave model, while the Stochastic Collision model is selected for the collision model. The zero model is utilized for depicting the internal temperature distribution of individual droplets.

Given the presence of the evaporation process, a component transport model is introduced to analyze changes in gas phase composition. In this regard, a single component, $C_{12}H_{23}$, is employed instead of aviation kerosene due to its complex composition.

Boundary conditions involve a no-slip condition for the wall surface, application of the standard wall function for the near-wall region, and implementation of the Lagrangian Wall-Film model for droplets in contact with the wall. It's important to note that the Wall-Film model assumes adiabatic wall surface conditions and does not consider the external environment's impact on fuel atomization and evaporation within the evaporator tube.

Boundary conditions

The air inlet is specified as a mass flow inlet, the fuel mass flow rate is 0.000333 kg/s, inlet gauge pressure 10000Pa, the inlet temperature is set at 430 K, and the inlet turbulence boundary condition prescribes a turbulence intensity of 5%. The Hydraulic Diameter is established at 5 mm. For the outlet, a free outlet outflow boundary condition is applied, reference pressure setting 310 kPa.

The wall boundary treatment designates stationary walls with no-slip conditions.

For the honeycomb sheet, the chosen material's physical parameters are provided in Table 4 physical parameters of honeycomb body.

Orthogonal design

To investigate the impact of honeycomb sheet shape and size parameters on the evaporator tube's performance, we employ the orthogonal test method within the framework of Design and Analysis of Experiments (DAE). Through this approach, a total of 9 scenarios are selected for numerical simulation analysis of the straight evaporator tube with a honeycomb sheet. The application of the orthogonal test method aims to streamline the number of numerical simulation experiments while enhancing the reliability of the derived analysis results regarding influencing factors.

For the current study, an $L_9(3^4)$ orthogonal table is utilized. Three honeycomb sheet shape control parameters are identified as influencing factors, each with three levels. The resultant scheme is outlined in Table 5. Here, A signifies the honeycomb sheet thickness, B denotes the diameter of the openings, and C represents the number of honeycomb sheets. Specific values are assigned to these parameters, where "A1" corresponds to a honeycomb sheet thickness of 0.5 mm, "A2" corresponds to a thickness of 1 mm, and so forth.

In terms of combining the influencing factors, Scheme a adopts the combination A1B1C1, signifying a honeycomb sheet thickness of 0.5 mm, opening diameter of 0.4 mm, and a single honeycomb sheet.

Selection of eigenfaces

To investigate the impact of flow characteristics on the evaporation and atomization performance parameters of fuel within the evaporation tube, a series of cross-sectional positions were chosen. These positions are located at x = 24, 18, 12, 6, 0, −6, −12, −18, −24 mm along the length of the tube, as illustrated in Figure 4F. Notably, the cross-section at x = 24 corresponds to the location of the nozzle outlet. This selection of cross-sectional positions allows for a comprehensive exploration of the evaporation and atomization dynamics within the evaporation tube.

The parameters examined in this article primarily involve the Sauter Mean Diameter (SMD) of fuel droplets and the fuel evaporation rate. For calculating droplet SMD, SMD is a metric that assesses the size distribution of particles or droplets, representing the diameter of an ideal

sphere with the same volume. SMD can be computed through various methods: 1. Volume average method; 2. Number-based method; 3. Mass-based method. In this article, SMD is calculated using the Volume average method. Typically, conducting an Euler Lagrangian multi-phase flow simulation is necessary. This entails establishing a discrete phase model (DPM) in Fluent, where material properties, flow conditions, DPM-related parameters, initial values, and boundary conditions are defined. Post-processing allows for direct derivation of the droplet diameter for each section using the volume average method, thereby obtaining the SMD for each section.

For calculating the fuel evaporation rate, it's important to understand that this refers to the speed at which a liquid transitions into a gaseous state. In scientific research, various methods can be employed to quantitatively measure this rate. Here are some commonly used quantitative techniques: 1. Mass loss method; 2. Optical method; 3. Heat transfer model; 4. Humidity measurement method; 5. Mass spectrometry; 6. Pressure change method. In this article, the evaporation rate is calculated using a mass loss method. This involves several steps: setting a mass transfer model, defining substance properties, selecting an appropriate evaporation model, establishing initial and boundary conditions, and analyzing simulation results through post-processing.

To summarize, the parameters scrutinized in this paper primarily involve the Sauter mean diameter (SMD) of fuel droplets and the fuel evaporation rate. The calculation of the droplet SMD is facilitated through numerical simulation software, allowing for the determination of SMD at specific positions along the tube.[37] Additionally, the fuel evaporation rate is quantified by analyzing numerical simulation data, determining the ratio of evaporated fuel to the total fuel quantity at each individual cross-sectional point.[38]

Comparison of the performance of evaporator tubes in different structural states

The calculated outcomes of the evaporator tubes for the nine distinct scenarios are presented in Table 6. A thorough analysis reveals that scenarios c, e, and g exhibit higher evaporation rates coupled with relatively lower air flow rates and elevated mean outlet temperatures. However, no significant correlation is observed with regard to the Sautelle mean diameter factor.

Scenarios c, e, and g exhibit a commonality in honeycomb sheet count, despite varying aperture diameters and sheet thicknesses. The impact of honeycomb sheet parameters on evaporation tube performance is studied using the orthogonal experimental method in DAE. The consistent honeycomb cell number in schemes c, e, and g aligns with the scientific nature of orthogonal experiments, minimizing the need for numerical simulations and ensuring reliable analysis. The honeycomb sheet count emerges as a crucial factor influencing both evaporation and air flow rates. Dataset computations indicate that a higher sheet count correlates with increased air flow resistance, enhancing turbulence and improving droplet atomization and evaporation efficiency within the tube.